UC Santa Barbara

Title

Seismic equivalents of volcanic jet scaling laws and multipoles in acoustics

Permalink

https://escholarship.org/uc/item/10v421zh

Journal

ISSN

Authors

Haney, Matthew M
Matoza, Robin S
Fee, David
et al.

Publication Date

DOI

Copyright Information

Peer reviewed

Seismic equivalents of volcanic jet scaling laws and multipoles in acoustics

Matthew M. Haney,[1] Robin S. Matoza,[2] David Fee[3] and David F. Aldridge[4]

[1]*Alaska Volcano Observatory, U.S. Geological Survey, Anchorage, AK 99508, USA* *Email: mhaney@usgs.gov*
[2]*Department of Earth Science and Earth Research Institute, University of California, Santa Barbara, CA 93106, USA*
[3]*Alaska Volcano Observatory, University of Alaska Fairbanks Geophysical Institute, Fairbanks, AK 99775, USA*
[4]*Sandia National Laboratories, Geophysics Department, Albuquerque, NM 87185, USA*

SUMMARY

We establish analogies between equivalent source theory in seismology (moment-tensor and single-force sources) and acoustics (monopoles, dipoles and quadrupoles) in the context of volcanic eruption signals. Although infrasound (acoustic waves < 20 Hz) from volcanic eruptions may be more complex than a simple monopole, dipole or quadrupole assumption, these elementary acoustic sources are a logical place to begin exploring relations with seismic sources. By considering the radiated power of a harmonic force source at the surface of an elastic half-space, we show that a volcanic jet or plume modelled as a seismic force has similar scaling with respect to eruption parameters (e.g. exit velocity and vent area) as an acoustic dipole. We support this by demonstrating, from first principles, a fundamental relationship that ties together explosion, torque and force sources in seismology and highlights the underlying dipole nature of seismic forces. This forges a connection between the multipole expansion of equivalent sources in acoustics and the use of forces and moments as equivalent sources in seismology. We further show that volcanic infrasound monopole and quadrupole sources exhibit scalings similar to seismicity radiated by volume injection and moment sources, respectively. We describe a scaling theory for seismic tremor during volcanic eruptions that agrees with observations showing a linear relation between radiated power of tremor and eruption rate. Volcanic tremor over the first 17 hr of the 2016 eruption at Pavlof Volcano, Alaska, obeyed the linear relation. Subsequent tremor during the main phase of the eruption did not obey the linear relation and demonstrates that volcanic eruption tremor can exhibit other scalings even during the same eruption.

Key words: Acoustic properties; Volcano seismology; Explosive volcanism; Volcano monitoring.

1 INTRODUCTION

Relating seismic and infrasonic signals generated during volcanic activity to eruption parameters is a fundamental challenge for volcano monitoring. Co-eruptive signals arise from the ejection of magmatic products from the vent and as a result should contain information on the eruption rate. Complicating matters is that many other types of seismic and infrasound signals can be generated during an eruption, including lahars (Zobin *et al.* 2009), pyroclastic flows (Yamasato 1997) and coupled waves from the air into the ground (Matoza & Fee 2014). In spite of these difficulties, a seismic signal known as volcanic eruption tremor is often identified in the band from 1–5 Hz during sustained eruptions and is interpreted in terms of the strength of the eruption (McNutt & Nishimura 2008).

Ichihara (2016) has given an extensive review of the state of scientific progress in relating seismic and infrasonic amplitudes to eruption rate. As summarized by Ichihara (2016), various au-thors have developed power-law models with seismic or acoustic squared-amplitude proportional to eruption rate raised to a particular exponent. The power-law exponents found by previous seismic and infrasonic studies have ranged from between 0.9 and 10 (Ichihara 2016). The wide range of variability throws into question which of these models is most accurate and under which conditions they apply. Early studies comparing tremor and eruption rate did so by extracting the maximum tremor amplitude and the highest plume measurement for a given eruption (McNutt 1994; Roach *et al.* 2001; Prejean & Brodsky 2011; Senyukov 2013). However, this approach undersamples the dynamics of a sustained eruption lasting hours or longer. Modern methods measure plume height with high temporal density (Arason *et al.* 2011; Petersen *et al.* 2012; Hreinsdóttir *et al.* 2014; Ichihara 2016; Fee *et al.* 2017a), and as a result obtain inferred estimates of eruption rate highly sampled in time, offering a means of improved comparisons with seismic and infrasonic data.

Eruption rates can be estimated from measurements of plume height using an empirical relation developed by Sparks *et al.* (1997) and improved by Mastin *et al.* (2009), which states that the rate of mass erupted per unit time, termed the mass eruption rate $\dot{m}$, is approximately proportional to the fourth power of volcanic plume height, $\dot{m} \propto H^4$. The eruption rate can also be expressed in terms of the dense rock equivalent (DRE) volume eruption rate $q_{DRE} = \dot{m}/\rho_{DRE}$, where ρ_{DRE} is taken to be a common density of crustal rocks (e.g. 2500–2700 kg m^{-3}). This quantity should not be confused with the true volume eruption rate q in terms of the plume density, $q = \dot{m}/\rho_p$, where ρ_p is the density of the plume [e.g. 1–5 kg m^{-3} (Kieffer 1977; Ogden *et al.* 2008; Caplan-Auerbach *et al.* 2010; Fee *et al.* 2017a,b)]. The true volume eruption rate is important when considering that it can be expressed in terms of the area of the vent A_v and the exit velocity v_e of the plume material through the relation $q = A_v v_e$. The DRE volume on the other hand, is important when comparing the amount of volcanic material erupted as tephra versus the volume extruded as lava flows.

In this paper, we seek to develop scaling laws for seismic tremor amplitude and eruption rate based on existing scaling laws between infrasonic tremor amplitude and eruption rate. Such theoretical scaling laws in volcano infrasound have a much longer history than in volcano seismology. This is due largely to the work of Woulff & McGetchin (1976), who popularized key results from acoustic analogy theory and dimensional analysis to link monopole, dipole, and quadrupole acoustic sources to jet velocity. Although Woulff & McGetchin (1976) considered audible acoustic signals from fumaroles at Acatenango Volcano, their results have subsequently been widely used by infrasound researchers. From the extensive literature review presented in Ichihara (2016), we infer that theoretical models relating short period (> 1 Hz) seismic tremor amplitude to eruption rate did not appear for effusive eruptions for almost 30 yr (Battaglia *et al.* 2005) and as many as 35 yr later for explosive eruptions (Prejean & Brodsky 2011). The delay between Woulff & McGetchin (1976) and these subsequent seismic studies follows from table 1 of Ichihara (2016). Regarding non-eruptive tremor, pioneering work by Aki *et al.* (1977) addressed flow properties and seismic amplitude of shallow tremor in the lower East Rift Zone of Kilauea volcano. Aki & Koyanagi (1981) related the amplitude of deep volcanic tremor at Kilauea to magma transport and its flow rate in the subsurface. For seismic long-period earthquakes (LPs) preceding an eruption at Redoubt Volcano, Chouet *et al.* (1994) showed how to estimate pressure within a fluid-driven crack from the amplitude of the LPs. Although non-eruptive tremor and precursory LPs are not strictly speaking co-eruptive phenomena, magma and fluid transport in the subsurface should have similarities with eruption processes at the vent. Empirical models relating seismic amplitude to proxies of eruption rate, such as lava fountain height and ash plume height, had already appeared by about 1990 (Eaton *et al.* 1987; McNutt 1994). Given these studies relating seismic amplitude and volume eruption rate, it is worth noting that empirical models have also been developed between the radiated seismic energy of earthquake activity prior to an eruption and intruded volume (White & McCausland 2016).

Although a wide range of power laws have been proposed for relationships between seismoacoustic amplitudes and eruption rate, Ichihara (2016) found that the mean squared amplitude of seismic and infrasonic tremor during the 2011 sub-Plinian eruption of Shinmoe-dake displayed a nearly linear scaling with eruption rate, especially during the growing or quasi-stable portion of the eruption. The linear scaling is on the low end of the range of power exponents suggested in previous studies (0.9–10). It is worth clarifying how seismic and infrasonic tremor amplitude is quantified before pro-

ceeding further. In volcano acoustics, the amplitude level has been traditionally measured as radiated power (Woulff & McGetchin, 1976), which is proportional to the mean square pressure within a time window. To compute the radiated power accurately, other variables must be known such as the mean square radiation pattern and any significant propagation effects. In volcano seismology, the most widely used measure of tremor amplitude is known as reduced displacement, D_R, which is proportional to the root-mean-square displacement in a time window. It follows that reduced displacement squared, D_R^2, is proportional to the mean square displacement. However, the rate of radiation of seismic energy, called the radiated seismic power, is proportional to the mean square velocity in a time window (Johnson & Aster 2005). This is an important distinction, but in practice it does not make a major difference whether one takes the mean square displacement or the mean square velocity of tremor. This has been pointed out by Ichihara (2016), who stated that 'using ground velocity gives essentially the same results' as using displacement. Consider the reduced ground velocity squared, V_R^2, which is calculated in the same way as reduced displacement squared but using ground velocity instead of displacement. One measure of the dominant frequency ω_d of tremor is the ratio of reduced ground velocity squared over reduced displacement squared, $\omega_d^2 = V_R^2/D_R^2$. If ω_d does not vary significantly over the duration of volcanic tremor, radiated seismic power is proportional to the square of the dominant frequency times the reduced displacement squared. Thus, in that case, reduced displacement squared and reduced ground velocity squared are both proportional to radiated seismic power. In this paper, we focus on the measure of tremor amplitude in terms of its radiated seismic and infrasonic power.

Ichihara (2016) points out that, in terms of seismic tremor, the observed linear scaling between seismic radiated power and eruption rate at Shinmoe-dake most closely agrees with the empirical scaling between reduced displacement of tremor and ash plume height by McNutt (1994). Since the relation by McNutt (1994) is empirical, this motivates the question of what physical model gives rise to such a linear relation. We begin to address this issue by first seeking analogies between seismic and acoustic sources at volcanoes. We make connections between seismic sources and equivalent acoustic sources as described by acoustic analogy theory (Lighthill 1963, 1978) and discover a fundamental property that involves explosion, torque, and force seismic sources. We move on to a discussion of relationships between volcanic eruption parameters that indicate volcanic eruptions display self-similarity, a concept that is invoked in the study of earthquakes (Kanamori & Anderson 1975) and has previously been recognized for volcanoes (Nishimura & Hamaguchi 1993) and volcanic jet noise (Matoza *et al.* 2009). We finally illustrate these concepts by analysing the scaling between radiated power of seismic eruption tremor and plume height during the 2016 eruption of Pavlof Volcano, Alaska.

2 SEISMIC ANALOGIES TO VOLCANIC INFRASOUND SCALING LAWS

We explore connections between the seminal work of Woulff & McGetchin (1976) on acoustic radiation from volcanoes and seismicity observed during eruptions. Woulff & McGetchin (1976) applied key results from acoustic analogy theory by Lighthill (1952, 1954, 1963, 1978) and Curle (1955) to monopole, dipole, and quadrupole sources of volcano acoustics. Woulff & McGetchin (1976) summarized these models with the following scaling laws:

$$W_M = K_M \frac{\rho_p A_v}{c} v_e^4 \qquad (1)$$

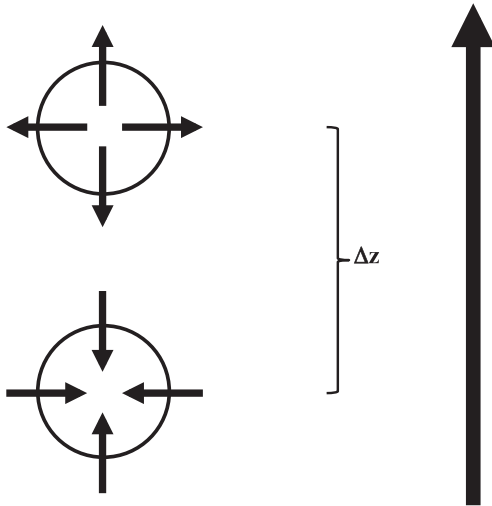Explosion/implosion pair (dipole)　=　Acoustic force source

Figure 1. The geometry for the combination of two monopoles of opposite sign, an explosion and an implosion, in order to produce an acoustic dipole in 2-D (Lighthill 1978). Whereas an acoustic monopole produces energy due to a time-varying mass flux, an acoustic dipole introduces no net mass and is equivalent to a force acting on the fluid.

$$W_D = K_D \frac{\rho_p A_v}{c^3} v_e^6 \qquad (2)$$

$$W_Q = K_Q \frac{\rho_p A_v}{c^5} v_e^8, \qquad (3)$$

where W_M, W_D and W_Q are radiated acoustic power from monopole, dipole, and quadrupole sources, respectively, ρ_p is the density of the plume or jet, A_v is the cross-sectional area of the vent, c is the speed of sound, v_e is the exit or flow velocity, and K_M, K_D and K_Q are dimensionless coefficients of proportionality called 'acoustic power coefficients' by Lighthill (1952, 1954). It is important to keep in mind that monopoles (time-varying mass fluxes) are the fundamental building block of equivalent sources in acoustics, as discussed by Kim *et al.* (2012) and Matoza *et al.* (2013). In Fig. 1, we show how an acoustic dipole is formed from a pair of monopoles of opposite sign. No net mass is introduced by the positive and negative monopoles, but together they impart a net force on the fluid. Similarly, an acoustic quadrupole is formed by two dipoles or equivalently four monopoles, with two of the monopoles being opposite in sign from the other two (Matoza *et al.* 2013).

In their application of acoustic analogy theory to volcano acoustics, Woulff & McGetchin (1976) also utilized the Strouhal number *St* (Kundu & Cohen 2008; Matoza *et al.* 2009; Fee & Matoza 2013), which relates frequency *f* to flow speed *U* and a characteristic length scale of *L*:

$$St = \frac{fL}{U} \qquad (4)$$

For a jet flow such as at the base of an eruption column, *U* is the expanded jet velocity (the flow velocity once the jet has equilibrated to atmospheric pressure) and *L* is the expanded jet diameter. Over a wide range of flow conditions, the Strouhal number can be considered constant (Woulff & McGetchin 1976) and, as a result, $fL \propto U$. In volcano seismology, the concept of the Strouhal number has not been as widely used as in infrasonic volcano studies, although a

notable exception is the work by Hellweg (2000). Chouet (1992) has also discussed the Strouhal number of magma flows that generate volcanic tremor. Within the field of volcano infrasound, estimating the Strouhal number of eruption plumes is an active area of research. McKee *et al.* (2017) have given an overview of Strouhal values obtained at several volcanoes. From field data shown in Matoza *et al.* (2009), the Strouhal number was estimated to be 0.4 at Tungarahua and 0.06 at Mount St. Helens. Cerminara *et al.* (2016) found the Strouhal number from a full-physics numerical simulation of a volcanic plume to be 0.32. Tam *et al.* (1996) calculated in a pure-air jet laboratory experiment that the Strouhal number approached 0.19 as the jet velocity decreased toward the ambient sound speed. Matoza *et al.* (2009) points out that these values for the Strouhal number fall into the range observed for man-made jets. Although the values of these Strouhal estimates vary, the theory we present in this paper does not depend on the Strouhal number being constant for all volcanoes. We only assume that the Strouhal number is a constant at a particular volcano. Thus, we are consistent with the assumption by Woulff & McGetchin (1976), wherein it was stated that the Strouhal number is often 'essentially constant over wide variations of flow conditions'. More details comparing the Strouhal number for man-made and volcanic jets can be found in Matoza *et al.* (2009) and Fee & Matoza (2013). In the following, we analyse seismic radiation from a force source and utilize the Strouhal number in eq. (4). The representation of the seismic source from a volcanic eruption as a force has been previously discussed by several authors (Kanamori *et al.* 1984; Nishimura & Hamaguchi 1993; Brodsky *et al.* 1999; Prejean & Brodsky 2011).

We begin by analysing the amount of seismic power radiated by a harmonic vertical force source applied at the surface of an elastic half-space. After fully discussing the case of a seismic force source, we later examine additional types of seismic sources, such as a moment source, and we show the analysis of these sources in Appendix A. Miller & Pursey (1955) analytically solved the problem of seismic power radiation from a vertical force for a Poisson's ratio of 0.25 and the solution is given as:

$$W = 4.836 \frac{\pi^3 f^2 a^4 P^2}{\rho \alpha^3}, \qquad (5)$$

where we have used their notation in which *W* is the radiated power of the seismic waves, *f* is the linear frequency (i.e., $2\pi f = \omega$), *a* is the radius of the circular area where the vertical force is applied, *P* is the force per unit area, ρ is the density of the solid half-space, and α is the *P*-wave velocity. Note that the total seismic power in this case is the sum of the power radiated as *P*-waves, *S*-waves and Rayleigh waves, although Rayleigh waves constitute approximately two-thirds of the total radiated power for a Poisson's ratio of 0.25 (Miller & Pursey 1955). The product $\pi^2 a^4 P^2$ is equal to the square of the circular area over which the force is applied times the squared force per unit area, so that it can be expressed concisely as the applied force squared F^2:

$$W = 4.836 \frac{\omega^2 F^2}{4\pi \rho \alpha^3}, \qquad (6)$$

where the result has been rewritten in terms of angular frequency ω. From eq. (6), we can see that the seismic power radiated by a force source is proportional to the following physical quantities:

$$W \propto \frac{\omega^2 F^2}{\rho \alpha^3}. \qquad (7)$$

In eq. (7), the numerical factor has been omitted for the purpose of studying scaling. It is determined by the Poisson's ratio of the

elastic half-space. We assume very minor variation in Poisson's ratio during eruptions or between different volcanoes, so its effect is not included in our analysis.

In their study of the relationship between eruption seismicity and plume height, Prejean & Brodsky (2011) showed how to express the applied force F in terms of the physical properties of a plume or jet acting at the surface of an elastic half-space. Following work by Brodsky *et al.* (1999) on very-long-period seismic waves generated by the 1980 Mount St. Helens eruption, Prejean & Brodsky (2011) put forward that the applied force is given by

$$F \propto q \rho_p v_e, \tag{8}$$

where q is the volume eruption rate, ρ_p is the density of the material in the plume or jet, and v_e is the exit velocity of the material. Note that we give the expression for the force source as a proportionality instead of the equality used in Prejean & Brodsky (2011). We do so because our emphasis, as shown in later sections, is on the exponent of the power law scaling relationship between radiated seismic power and eruption rate. The constant of proportionality is not the focus of this study, and it would be much more difficult to obtain from first principles. On the other hand, insight into the exponent of the power law scaling can be gained from theory as we demonstrate. The expression for the force source may approach equality at very long periods; however, we consider a harmonic force with a frequency in the range of 1 Hz, as commonly observed for volcanic eruption tremor. As a result, the oscillating component of the force in this higher frequency range is only proportional to the product of mass eruption rate and exit velocity. An equality could be derived over all frequencies by considering aspects such as the rolloff of the force source spectrum and coupling between the plume and the solid Earth, but these aspects are beyond the scope of this study. We illustrate the issue of proportionality versus equality in the expression of the source later by applying a similar analysis to the earthquake moment source.

Typically, the volume eruption rate can be further expressed as the product of the vent area A_v and the exit velocity, $q = A_v v_e$, which gives

$$F \propto A_v \rho_p v_e^2. \tag{9}$$

Substituting this into eq. (7) gives:

$$W \propto \frac{\omega^2 A_v^2 \rho_p^2 v_e^4}{\rho \alpha^3} \tag{10}$$

which shows the v_e^4 scaling of this model as previously pointed out by Ichihara (2016) and referred to as the 'fourth power law'. Rearranging terms, eq. (10) can be rewritten as

$$W \propto \frac{\rho_p A_v v_e^4}{\alpha^3} \left(\frac{A_v \rho_p \omega^2}{\rho} \right). \tag{11}$$

As was done in the seminal paper by Woulff & McGetchin (1976), we now appeal to the concept of the Strouhal number and take the ratio $\omega \sqrt{A_v}/v_e$ as a constant over a wide range of flow conditions, yielding:

$$W \propto \frac{\rho_p A_v v_e^6}{\alpha^3} \left(\frac{\rho_p}{\rho} \right). \tag{12}$$

In contrast to the fourth power law in velocity implied by eq. (10), we see that the force model by Prejean & Brodsky (2011) actually leads to a sixth power law in velocity when taking into account flows characterized by a Strouhal number. The scaling based on the sixth power is equivalent to the relation developed by Curle (1955) and applied by Woulff & McGetchin (1976) for *dipole* acoustic sound

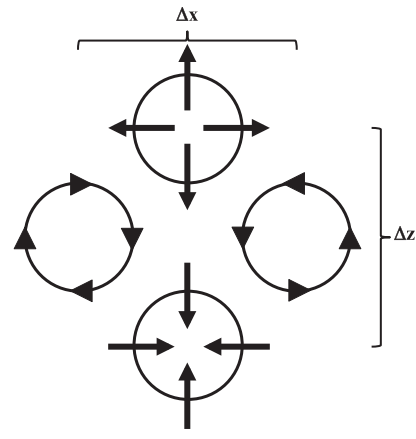Explosion/implosion pair + Torque/anti-torque pair   =   Seismic force source

Figure 2. The geometry for the combination of explosion and torque dipoles required to reproduce a seismic force source in 2-D.

radiation, as shown in eq. (2). Therefore, in the seismic case, a force acting on the surface of a half-space produces the same scaling as dipole sound radiation. Note the additional factor of ρ_p/ρ in eq. (12) compared to the sixth-power-law for dipole radiation by Woulff & McGetchin (1976). This factor expresses the coupling of the plume or jet to the solid half-space in the seismic case.

The fact that the scaling law shows a seismic force source has the same scaling as an acoustic dipole requires some clarification. In seismology, forces are considered to be the fundamental building blocks of sources. This is the basis of the equivalent force system in the construction of moment tensors, where individual moments are represented by force couples and dipoles. For example, Kanamori & Given (1982) have referred to the horizontal force source during the 1980 Mount St. Helens eruption as a terrestrial monopole, in the sense that it was a force monopole instead of a force dipole. However, in Appendix B, we show that a seismic force can be represented by dipoles of explosive sources that only radiate *P*-waves and torque sources that only radiate *S*-waves. Thus, it makes sense that the preceding analysis showed a force source has the same scaling as an acoustic dipole. The geometry of the dipoles needed to reproduce a force source in 2-D is shown in Fig. 2: the dipole consisting of an explosion/implosion pair is oriented along the direction of the force and the torque dipole is oriented perpendicular to the force direction. As shown in Fig. 1, this geometry is similar to how a dipole source is formed in acoustics from two closely spaced acoustic monopoles of opposite polarity (Pierce 1989; Russell 1999; Kim *et al.* 2012; Matoza *et al.* 2013). However, in the seismic case, the presence of the additional *S*-wave mode requires the presence of the torque sources as well to reproduce a seismic force. The relation depicted in Fig. 2 is a fundamental property of seismic sources that brings together explosion, torque, and force sources, the latter two being types of sources normally ignored in seismic source inversions (Takei & Kumazawa 1994). In the same way as the equivalent force system is a decomposition of a moment tensor source into force couples and dipoles, we have shown here that a seismic force source can be further decomposed into explosion and torque dipoles. Although Fig. 2 is for 2-D, the equivalence can also be extended to 3-D as well, as described in Appendix B. The arrangement of the dipoles needed to replicate a force source in 3-D is shown in Fig. 3. In this case, the presence of an added dimension compared to the 2-D case requires a second set of torque dipoles arranged along the other axis perpendicular to the force direction. As shown in Appendix B,
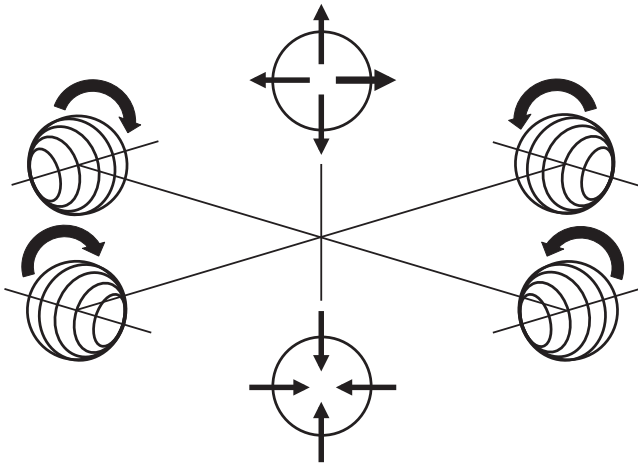
Figure 3. The geometry for the combination of explosion and torque dipoles required to reproduce a seismic force source in 3-D.
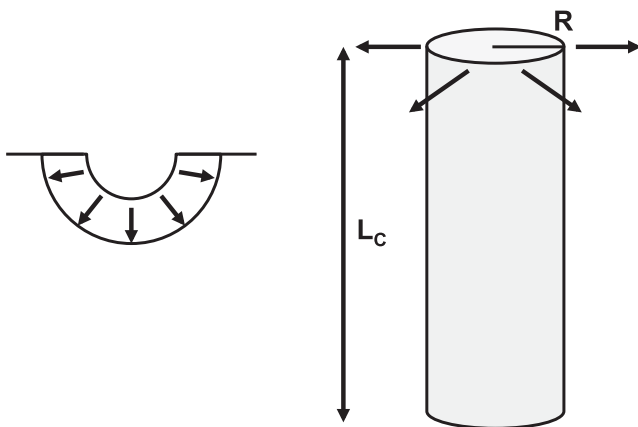

Figure 4. Seismic analogies of monopole (left) and quadrupole (right) sources. The monopole analogy is taken to be an expanding cavity of volume injection into the elastic half-space. The quadrupole analogy is based on the moment tensor model of McNutt & Nishimura (2008) in which turbulence is excited over a volume within the conduit of length L_C and radius R.

this geometry of dipoles reproduces the wave field of a seismic force source in 3-D when the dipoles are brought infinitely close together. Notably, in this limit the wave field is azimuthally symmetric with respect to the direction of the force source. Following up on these developments for a seismic force source and dipole scaling, we extend the dimensional analysis to cover the other two types of fundamental acoustic sources: monopoles and quadrupoles. The derivations for these cases are given in Appendix A and we summarize the results here. We find the seismic analogy of an acoustic monopole source, which displays fourth-power scaling with exit velocity as in eq. (1), is given by a seismic source of volume injection as described by Aldridge (2002). At a volcano, the volume injection source is depicted as a hemispherical crater expanding into the subsurface, as shown in Fig. 4. The analogy of an acoustic quadrupole source, which displays eighth-power scaling with exit velocity as in eq. (3), is given by a moment tensor seismic source. For example, McNutt & Nishimura (2008) propose a moment tensor source to represent eruption tremor caused by turbulence within a conduit. In Appendix A, we show how their source leads to quadrupole-like scaling. The geometry of the seismic analogy of a quadrupole source is shown in Fig. 4, and the turbulence is assumed to be excited along a particular length of the shallow conduit L_C.

3 SCALING THEORY FOR VOLCANIC ERUPTIONS

In the previous section we made connections between well-known scaling laws in volcano infrasound and models of volcanic seismicity. Here we take the analysis a step further and examine the applicability to volcanic eruptions. We consider additional relationships among volcano parameters such as the area of the vent, exit velocity, and pressure in the magma reservoir and derive a complete scaling theory for volcanoes that is similar to existing earthquake scaling laws. To make the analogy with earthquake scaling laws clear, we simultaneously show normal earthquake scaling theory using similar notation. The analysis builds on the volcano scaling relations derived by Nishimura & Hamaguchi (1993). Our primary motivation is to investigate physical models to explain the observed linear scaling between radiated seismic power and eruption rate (McNutt 1994; Ichihara 2016). The observations of linear scaling are surprising given that the scaling of a seismic force described in the previous section is to the sixth power in terms of eruption rate (i.e. to the sixth power of exit velocity). In spite of such a large apparent discrepancy between theory and observations, we show in this section that a linear scaling is predicted by the theory when other relationships between eruption parameters are invoked and these relationships have been previously discussed by Nishimura & Hamaguchi (1993).

One of the well-known outcomes of earthquake source scaling is that radiated energy and moment are proportional to each other (Stein & Wysession 2003). In the following, we show this for earthquakes and apply a similar analysis to volcanic eruption seismicity. We assume the vertical force source model discussed previously for a volcanic eruption and shown in eq. (9):

$$F \propto \rho_p A_v v_e^2,$$

where ρ_p is the density of the plume or jet, A_v is the area of the vent, and v_e is the exit velocity. For earthquakes, the moment rate source is given by

$$\dot{M} \propto \mu A_f v_s, \tag{13}$$

where μ is the shear modulus, A_f is the fault area, and v_s is the slip velocity. Similar to the expression for the volcanic force source, the earthquake moment source is given as a proportionality instead of an equality. The seismic moment is the low-frequency asymptote of the seismic spectrum in the standard earthquake model. For a higher frequency, oscillating component of the moment source, as considered here, the moment release will be less than that asymptote. The frequency-dependent, dimensionless factor that would render eq. (13) an equality follows from the rolloff of the earthquake source spectrum. Since here we are only interested in the exponent of power-law relations between volcano and earthquake source parameters, and not the constant of proportionality, the fact that we use proportionalities instead of equalities to describe the force and moment sources does not affect the final results. From the expressions showing the proportionality of volcanic force and earthquake moment sources to their respective parameters, we can examine their radiated seismic power. The radiated power for a force source scales as already shown in eq. (7):

$$W \propto \frac{\omega^2 F^2}{\rho \alpha^3},$$

where W is the radiated power, F is the magnitude of the force, ω is angular frequency, ρ is the density of the solid half-space, and α is the P-wave velocity. Note that, as in the previous section, we do not

include Poisson's ratio in the scaling relation. The radiated power for a moment source scales as (Rose 1984)

$$W \propto \frac{\omega^2 \dot{M}^2}{\rho \beta^5}, \tag{14}$$

where $\dot{M}$ is the magnitude of the moment rate source and β is the shear wave velocity.

Before we insert eq. (9) into eq. (7) and eq. (13) into eq. (14), there are some additional relations for earthquakes and volcanic eruptions that we need to consider. For volcanic eruptions, we assume as discussed earlier that the flow of material out of the vent is characterized by a constant Strouhal number (Woulff & McGetchin 1976) such that

$$\omega \propto \frac{v_e}{\sqrt{A_v}}. \tag{15}$$

For earthquakes, a similar relation holds between the corner frequency ω_c, the S-wave velocity, and the area of the fault (Kanamori & Anderson 1975; DelPezzo *et al.* 2013):

$$\omega_c \propto \frac{\beta}{\sqrt{A_f}}, \tag{16}$$

where we assume the rupture velocity is proportional to the shear wave velocity β. A majority of the energy radiated by an earthquake is radiated near the corner frequency, so in the following relationships for radiated energy we only consider that frequency. Another relation exists for earthquakes between the moment, fault area and stress drop $\Delta\sigma$ (Kanamori & Anderson 1975):

$$A_f^{3/2} \propto \frac{M}{\Delta\sigma}. \tag{17}$$

The analogy of this equation for volcanic eruptions has been discussed before by Nishimura & Hamaguchi (1993) and is given by

$$A_v \propto \frac{F}{\Delta P}, \tag{18}$$

where ΔP is the excess pressure in the magma reservoir prior to the eruption. We emphasize that eq. (18) is a proportionality and not an equality. The proportionality factor is related to the relative shape of the magma reservoir and vent. For example, the simplified eruption model of Kanamori *et al.* (1984) would have a proportionality factor of 6 on the right-hand side of eq. (18) since the eruption takes place through one side of cube. A third relation that exists for earthquakes states that the strain release $\Delta\sigma/\mu$ is constant. This means that stress drop and shear modulus scale with each other (Kanamori & Anderson 1975):

$$\Delta\sigma \propto \mu. \tag{19}$$

The analogy of this relation for volcanic eruptions is that the excess pressure scales with the longitudinal modulus:

$$\Delta P \propto \lambda + 2\mu, \tag{20}$$

where λ is Láme's first parameter. In eq. (20), we have assumed a simple 1-D vertical stress field in which a sill-like magma reservoir is in a state of uniaxial strain. This relation is supported by the conclusions of Nishimura & Hamaguchi (1993), who found that the excess pressure in a magma reservoir prior to an eruption was 1 MPa with a variation of only one order of magnitude. Since bulk longitudinal modulus should not vary greatly in the shallow crust, eq. (20) implies that ΔP should also not vary greatly.

We combine the above relations to produce forms that will be useful in the analysis of radiated seismic energy. Beginning with

earthquakes, if we insert eq. (17) into eq. (16), we obtain the following scaling:

$$M\omega_c^3 \propto \beta^3 \Delta\sigma. \tag{21}$$

Near the corner frequency, where most earthquake energy is radiated, this can be expressed in terms of moment rate instead of moment:

$$\dot{M}\omega_c^2 \propto \beta^3 \Delta\sigma. \tag{22}$$

Inserting the expression for moment rate given in eq. (13) yields

$$\mu A_f v_s \omega_c^2 \propto \beta^3 \Delta\sigma. \tag{23}$$

We now use the relation in eq. (16) to rewrite the above expression as

$$\mu v_s \propto \beta \Delta\sigma, \tag{24}$$

which can be rearranged to isolate strain release on the right-hand side:

$$\frac{v_s}{\beta} \propto \frac{\Delta\sigma}{\mu}. \tag{25}$$

This equation means the slip velocity is proportional to the S-wave velocity, under the assumption of constant strain release.

Moving on to volcanic eruptions, if we insert eq. (18) into eq. (15), we obtain the following scaling:

$$F\omega^2 \propto v_e^2 \Delta P. \tag{26}$$

Inserting the expression for the vertical force source given in eq. (9) yields

$$A_v \rho_p \omega^2 \propto \Delta P. \tag{27}$$

We now use the relation in eq. (15) to rewrite the above expression as

$$\rho_p v_e^2 \propto \Delta P. \tag{28}$$

This expression states that the dynamic pressure of the flow at the vent scales with the excess pressure in the magma reservoir prior to the eruption. It can be rewritten as

$$\frac{v_e^2}{\alpha^2}\left(\frac{\rho_p}{\rho}\right) \propto \frac{\Delta P}{\lambda + 2\mu}. \tag{29}$$

The right-hand side of this equation is assumed to be constant according to eq. (20) and therefore it implies a proportionality between the exit velocity, the P-wave velocity of the solid half-space, and the ratio of the plume density to the density of the solid half-space.

In light of these results, we now analyse scaling for volcanic eruptions and earthquakes. We start with earthquakes since the result is well known. Substituting eq. (13) into eq. (14), and also using the relation in eq. (16) gives the following expression for radiated power:

$$W \propto \frac{\mu A_f v_s^2}{\beta}. \tag{30}$$

Writing this eq. in terms of the moment rate using eq. (13) yields

$$W \propto \dot{M}\frac{v_s}{\beta}. \tag{31}$$

However, as shown in eq. (25), the ratio of slip velocity to the S-wave velocity is considered constant, so that power scales with moment rate: $W \propto \dot{M}$. Power is simply energy rate, so this means that energy rate scales with moment rate or, as more commonly stated, that energy and moment are proportional to each other in

the standard model for earthquakes. For volcanoes, substituting eq. (9) into eq. (7), and also using the relation in eq. (15), gives the following expression for radiated power:

$$W \propto \frac{\rho_p A_v v_e^6}{\alpha^3} \left(\frac{\rho_p}{\rho} \right). \tag{32}$$

As pointed out previously, this has the same form as the dipole acoustic model for volcanic plumes discussed by Woulff & McGetchin ([1976](#)). Writing this equation in terms of the force source using eq. (9) yields

$$W \propto F \frac{v_e^4}{\alpha^3} \left(\frac{\rho_p}{\rho} \right). \tag{33}$$

However, as shown in eq. (29), the quantity $v_e^2 \rho_p / \alpha^2 \rho$ is considered constant, so that the radiated energy can be simplified as

$$W \propto F \frac{v_e^2}{\alpha}. \tag{34}$$

This is the analogy of $W \propto \dot{M}$ for volcanic eruptions described by the relations shown above.

In their eq. 13, Nishimura & Hamaguchi ([1993](#)) show that the energy for an explosion earthquake at a volcano scales as

$$E \propto R^3 P_0, \tag{35}$$

where R is the radius of the vent and P_0 is the pressure in the reservoir prior to eruption. In terms of radiated power instead of energy, this relation is given by

$$W \propto \omega R^3 P_0, \tag{36}$$

where ω is the frequency. Nishimura & Hamaguchi ([1993](#)) point out that, similar to eq. (20), the pressure in the reservoir prior to an eruption does not vary greatly for different eruptions. This is analogous to how stress drop does not vary greatly for earthquakes over many orders of magnitude. As a result, Nishimura & Hamaguchi ([1993](#)) conclude that the energy release of a volcanic explosion earthquake is primarily determined by its crater radius R^3. For earthquakes, this same argument means earthquake size is determined by the area of the fault.

We now put our result in eq. (34) in context with the scaling found by Nishimura & Hamaguchi ([1993](#)). By using eqs (15) and (18), we can rewrite eq. (34) as

$$W \propto \omega A_v^{3/2} \Delta P \frac{v_e}{\alpha}, \tag{37}$$

which is observed to have a similar form as eq. (36) with $A_v^{3/2} \propto R^3$ and $P_0 \propto \Delta P$. There is one significant difference, however, which is the additional non-dimensional parameter we have found: v_e/α, the ratio of the exit velocity to the P-wave velocity of the subsurface. We note that this ratio can also be considered as a Mach number in the solid. This factor does not appear in the original study by Nishimura & Hamaguchi ([1993](#)). The proportionality with exit velocity shows that the seismic power of tremor W scales linearly with eruption rate, if the excess pressure in a reservoir prior to an eruption is assumed to be nearly constant. Lack of variability in excess pressure prior to an eruption is an integral part of the scaling theory discussed by Nishimura & Hamaguchi ([1993](#)). The prediction of linear scaling agrees with observations of volcanic tremor reported by McNutt ([1994](#)), and the results from the 2011 Shinmoe-dake eruption (Ichihara [2016](#)), especially during the growing or quasi-stable portion of the eruption. The fact that the earthquake-like scaling discussed by Nishimura & Hamaguchi ([1993](#)) for volcanic explosion earthquakes leads to a linear relationship between seismic power

and eruption rate is consistent with the interpretation by Ichihara ([2016](#)) that sustained sub-Plinian volcanic eruptions can be considered a series of successive explosions. It remains to be seen whether other models, such as ones describing high-velocity conduit flow and fragmentation, also lead to a similar linear scaling. The linear scaling with eruption rate in eq. (37) is much different than the apparent sixth power scaling in eq. (32). This is due to the additional scaling relationships for volcanic eruptions that we have discussed in this section. Thus, the apparent sixth power scaling in eq. (32) is due to an incomplete scaling theory, one in which the dynamic similarity of flows with a constant Strouhal number has been taken into account, but not the additional similarity implied by excess pressure ΔP prior to an eruption scaling with bulk longitudinal modulus of the subsurface.

The idea that eruption tremor is made up of successive explosions, however, disagrees with the observation of different scaling for tremor and explosion earthquake energies versus vent radius discussed by McNutt & Nishimura ([2008](#)). We do not have a full explanation for this in terms of all the data shown in McNutt & Nishimura ([2008](#)), but we can comment on one of the data points shown from Pavlof Volcano, Alaska. An explosion earthquake occurred at Pavlof in 1988 with an estimated magnitude of $M_L = 2.5$ (Nishimura [1998](#)). McNutt & Nishimura ([2008](#)) convert tremor reduced displacement at Pavlof to equivalent magnitude and find a much lower magnitude value for the tremor, approximately $M_L = 0$. The same discrepancy is observed between tremor and explosion earthquakes at many volcanoes and leads to the observed difference in scaling reported by McNutt & Nishimura ([2008](#)). However, it is not possible to relate maximum reduced displacement directly to magnitude (or energy release) since reduced displacement does not take into account the duration of tremor (Kumagai *et al.* [2015](#)). In fact, cumulative tremor energy from several recent eruptions at Pavlof has been calculated over time windows that span the entire eruption and the equivalent magnitude is roughly equal to $M_L = 2.0$ (Waythomas *et al.* [2014](#)), close to the magnitude value of the explosion earthquake in 1988. Thus, we suggest the different scaling for tremor and explosion earthquake energies versus vent radius discussed in McNutt & Nishimura ([2008](#)) may be an artefact of converting reduced displacement to magnitude. The particular case of Pavlof points to tremor and explosion earthquakes releasing a similar amount of cumulative energy and, based on the observation of a linear relation between radiated power of tremor and eruption rate (McNutt [1994](#); Ichihara [2016](#)), we expect that tremor composed of successive explosions obeys the scaling relation in eq. (37). We further discuss Pavlof Volcano in the next section of this paper.

4 CO-ERUPTIVE TREMOR AT PAVLOF VOLCANO

We examine the scaling arguments we have described by analysing eruption tremor and plume heights during the 2016 eruption of Pavlof Volcano, located along the Alaska Peninsula and one of the most active volcanoes in the Alaska-Aleutian arc. On 2016 March 27, Pavlof began a significant eruption with little precursory activity. The strongest phase of the eruption occurred during the first 17 hr and was characterized by intense continuous tremor, lava fountaining, and an ash plume attached to the vent that extended over 800 km to the northeast (Fee *et al.* [2017a](#)). The eruption tremor was measured on a local network of five short period seismometers, each with a lower corner frequency of 1 Hz. Plume heights were
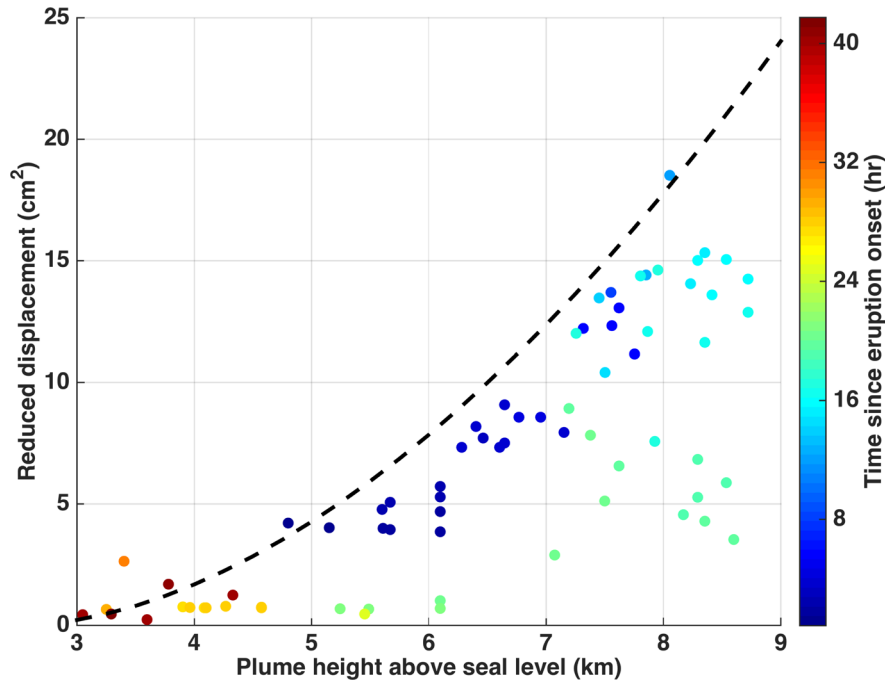
Figure 5. Plume height versus reduced displacement during the 2016 eruption of Pavlof Volcano. The dashed line is the empirical relation of McNutt (1994). The tremor reduced displacement closely agrees with the empirical relation over the first 17 hr of the eruption.

calculated by both satellite data and a web camera located 60 km away in Cold Bay, Alaska.

In Fig. 5, we cross-plot reduced displacement (D_R) of tremor against plume heights measured with the web camera and satellite data (Fee *et al.* 2017a). Approximately 17 hr into the eruption, Fee *et al.* (2017a) found that the character of the tremor-plume relationship changed. This can be seen in Fig. 5 where the time history trajectory in the D_R/plume-height plane 17 hr into the eruption begins to move below its initial trajectory. For example, in Fig. 5 the green data points (20 hr into the eruption) plot beneath the blue data points (8 hr into the eruption). This pattern means the ash plume height at late stages of the eruption remained at high altitudes even though the tremor level had fallen. Note that the ash plume remained attached to the vent during this entire time period. Fee *et al.* (2017a) interpreted this pattern in terms of hysteresis encountered in the emerging field of fluvial seismology and implicated erosion of the crater as the cause of the change in the trajectory.

We focus here on the first 17 hr of the eruption and compare the observed plume heights to the empirical relation between tremor reduced displacement D_R and plume height H derived by McNutt (1994):

$$\log_{10} D_R = 1.80 \log_{10} H - 0.08, \tag{38}$$

where D_R is in cm^2 and H is in km above the vent. Ichihara (2016) has pointed out that the relation by McNutt (1994) implies a nearly linear relationship between radiated seismic power and eruption rate, $W \propto q$. Since D_R is proportional to the square root of radiated power and eruption rate is proportional to the fourth power of plume height (Sparks *et al.* 1997; Mastin *et al.* 2009), a linear scaling between radiated seismic power and eruption rate translates into a quadratic relation between D_R and plume height, $D_R \propto H^2$. Such a quadratic relation with a power-law exponent of 2 is close to the value of 1.8 obtained by McNutt (1994) in eq. (38), which in turn corresponds to seismic power scaling with eruption rate with a nearly linear exponent of 0.9. In Fig. 5, the tremor during the first 17 hr of the

eruption is observed to reasonably follow the empirical relation by McNutt (1994), and this is additional evidence that radiated seismic power from tremor during sustained explosive eruptions, especially during the slowly growing stage (Ichihara 2016), scales with eruption rate. Note that the plume heights in Fig. 5 are plotted as height above sea level, whereas the relevant quantity is height above the vent (McNutt 1994; Sparks *et al.* 1997; Mastin *et al.* 2009). It is worth noting that Fee *et al.* (2017a) also analysed infrasonic tremor from the Pavlof eruption and found a similar pattern as shown for the seismic data in Fig. 5. This suggests that the seismic and infrasonic tremor, when cross plotted, show a linear relation with each other. Such a linear relation has also been observed between seismic and infrasonic tremor during the 2011 Shinmoe-dake eruption and has been interpreted as due to the tremor originating from a common, seismoacoustic source near the fragmentation level (Ichihara 2016).

We plot the tremor-plume data again in Fig. 6, but using log-log axes to highlight power-law relations. The red dashed line in Fig. 6 is a power-law fit to the data over the first 17 hr of the eruption and its slope is almost identical to the empirical relation by McNutt (1994) shown as a black dashed line. The only appreciable difference is that the Pavlof data is shifted slightly lower in terms of reduced displacement for a given plume height compared to the empirical relation. This difference corresponds to the constant factor being closer to −0.2 in eq. (38) for the Pavlof data rather than the value of −0.08 in the empirical relation. However, this difference is likely not significant given common uncertainties in the data. The more dramatic difference is shown by the blue dashed line in Fig. 6, which is the power-law fit to the data from 17–21 hr after the start of the eruption. The power-law exponent in this case is larger than the value of 1.8 in eq. (38) and the fit indicates it is close to a value of 3.5. At this point, it is not clear whether this change in scaling during the late portion of the eruption can be modelled in terms of a different type of seismoacoustic source. Based on the preceding theory, the larger power-law exponent may signify that the eruption seismicity shifted to a source better described by a moment tensor,
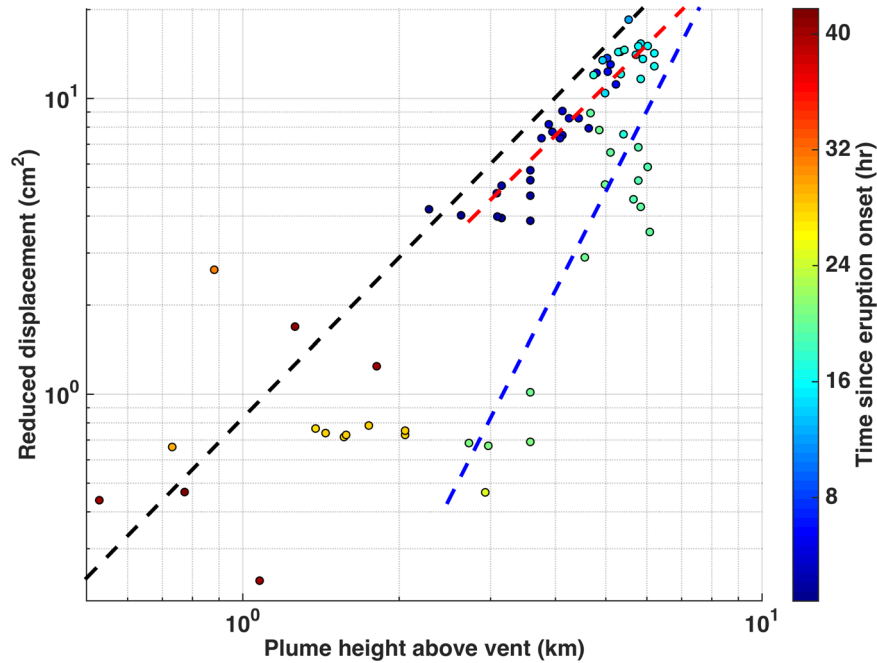
Figure 6. Same as Fig. 5 but plotted with log–log axes to highlight power laws. The dashed line is the relation of McNutt (1994), $D_R = 10^{-0.08}H^{1.8}$. A power-law fit to the first 17 hr of eruption tremor is shown as a dashed red line and is given by $D_R = 10^{-0.2}H^{1.7}$. The blue dashed line is a power-law fit to the eruption tremor between 17–21 hr after the eruption began and is given by $D_R = 10^{-1.7}H^{3.5}$.

such as the model of turbulence within the conduit by McNutt & Nishimura (2008) and discussed in Appendix A. However, this interpretation is outside the scope of this paper and will be addressed in the future by formulating a model for the changes at Pavlof due to crater erosion discussed in Fee *et al.* (2017a). The main result we find is that the linear scaling between seismic tremor power and plume height is obeyed over the first 17 hr of the eruption, and may represent a standard type of scaling observed generally for sustained sub-Plinian eruptions (McNutt & Nishimura 2008; Ichihara 2016).

5 CONCLUSIONS

We have made connections between common source representations used in seismology and infrasound in the context of volcanic eruption signals. We showed that monopole, dipole, and quadrupole sources of volcanic infrasound are analogous to seismicity radiated by volume injection, force, and moment sources, respectively, in terms of their scaling properties with eruption rate. We also proved a fundamental relationship that ties together explosion, torque, and force sources in seismology and highlights the underlying dipole nature of seismic forces. The representation of a force source in terms of dipoles of explosion and torque sources is a decomposition similar to the equivalent force system representation of a moment tensor. It suggests that explosion and torque sources can each be considered seismic monopoles of *P*- and *S*-wavefields, respectively. We built on the fourth-, sixth-, and eighth-power scaling results for seismic eruption tremor by describing additional relationships between eruption parameters that constitutes a complete scaling theory similar to the theory of earthquake scaling. Incorporation of these additional relations within the force source model of a volcanic eruption led to a linear scaling between radiated seismic power of tremor and eruption rate. We observe such a linear dependence during the first 17 hr of the 2016 Pavlof eruption. Subsequent tremor at the late stages of the Pavlof eruption does not display

a linear scaling and requires additional modelling in the future to understand its source process.

REFERENCES

Aki, K. & Koyanagi, R., 1981. Deep volcanic tremor and magma ascent mechanism under Kilauea, Hawaii, *J. geophys. Res.,* **86,** 7095–7109.

Aki, K., Fehler, M. & Das, S., 1977. Source mechanism of volcanic tremor: fluid driven crack models and their application to the 1963 Kilauea eruption, *J. Volcanol. Geotherm. Res.,* **2,** 259–287.

Aldridge, D.F., 2002. Elastic wave radiation from a pressurized spherical cavity, Technical Report SAND2002-1882, Sandia National Laboratories.

Arason, P., Petersen, G.N. & Bjornsson, H., 2011. Observations of the altitude of the volcanic plume during the eruption of Eyjafjallajökull, April-May 2010, *Earth Syst. Sci. Data,* **3,** 9–17.

Battaglia, J., Aki, K. & Staudacher, T., 2005. Location of tremor sources and estimation of lava output using tremor source amplitude on the Piton de la Fournaise Volcano: 2, Estimation of lava output, *J. Volcanol. Geotherm. Res.,* **147,** 291–308.

Ben-Menahem, A. & Singh, S.J., 1981. *Seismic Waves and Sources,* Springer-Verlag, New York.

Brodsky, E.E., Kanamori, H. & Sturtevant, B., 1999. A seismically constrained mass discharge rate for the initiation of the May 18, 1980 Mount St. Helens eruption, *J. geophys. Res.,* **104,** 29 387–29 400.

Caplan-Auerbach, J., Bellesiles, A. & Fernandes, J.K., 2010. Estimates of eruption velocity and plume height from infrasonic recordings of the 2006

eruption of Augustine Volcano, Alaska, *J. Volcanol. Geotherm. Res.,* **189,** 12–18.

Cerminara, M., EspostiOngaro, T. & Neri, A., 2016. Large Eddy Simulation of gas-particle kinematic decoupling and turbulent entrainment in volcanic plumes, *J. Volcanol. Geotherm. Res.,* **326,** 143–171.

Chouet, B., 1992. A seismic model for the source of long-period events and harmonic tremor, in *Volcanic Seismology. IAVCEI Proceedings in Volcanology,* Vol. 3, pp. 133–156, eds Gasparini, P., Scarpa, R. & Aki, K., Springer.

Chouet, B.A., Page, R.A., Stephens, C.D., Lahr, J.C. & Power, J.A., 1994. Precursory swarms of long-period events at Redoubt Volcano (1989-1990), Alaska: their origin and use as a forecasting tool, *J. Volcanol. Geotherm. Res.,* **62,** 95–135.

Curle, N., 1955. The influence of solid boundaries upon aerodynamic sound, *Proc. R. Soc. A,* **231,** 505–514.

DelPezzo, E., Bianco, F. & Borgna, I., 2013. Magnitude scale for LP events: a quantification scheme for volcanic quakes, *Geophys. J. Int.,* **194,** 911–919.

Eaton, J.P., Richter, D.H. & Krivoy, H.L., 1987. Cycling of magma between the summit reservoir and Kilauea Iki lava lake during the 1959 eruption of Kilauea volcano, in *Volcanism in Hawaii,* Vol. 2, pp. 1307–1335, eds Decker, R.W., Wright, T.L. & Stauffer, P.H., U.S. Geol. Surv. Prof. Pap. 1350.

Fee, D. & Matoza, R.S., 2013. An overview of volcano infrasound: from Hawaiian to Plinian, local to global, *J. Volcanol. Geotherm. Res.,* **249,** 123–139.

Fee, D., Haney, M.M., Matoza, R.S., VanEaton, A.R., Cervelli, P., Schneider, D.J. & Iezzi, A.M., 2017a. Volcanic tremor and plume height hysteresis from Pavlof Volcano, Alaska, *Science,* **355,** 45–48.

Fee, D. *et al.*, 2017b. Eruption mass estimation using infrasound waveform inversion and ash and gas measurements: Evaluation at Sakurajima Volcano, *Earth planet. Sci. Lett.,* **480,** 42–52.

Hellweg, M., 2000. Physical models for the source of Lascar's harmonic tremor, *J. Volcanol. Geotherm. Res.,* **101,** 183–198.

Hreinsdóttir, S. *et al.*, 2014. Volcanic plume height correlated with magma-pressure change at Grímsvötn Volcano, Iceland, *Nat. Geosci.,* **7,** 214–218.

Ichihara, M., 2016. Seismic and infrasonic eruption tremors and their relation to magma discharge rate: a case study for sub-Plinian events in the 2011 eruption of Shinmoe-dake, Japan, *J. geophys. Res.,* **121,** 7101–7118.

Johnson, J.B. & Aster, R.C., 2005. Relative partitioning of acoustic and seismic energy during Strombolian eruptions, *J. Volcanol. Geotherm. Res.,* **148,** 334–354.

Kanamori, H. & Anderson, D.L., 1975. Theoretical basis of some empirical relations in seismology, *Bull. seism. Soc. Am.,* **65,** 1073–1095.

Kanamori, H. & Given, J.W., 1982. Analysis of long-period seismic waves excited by the May 18, 1980, eruption of Mount St. Helens - a terrestrial monopole?, *J. geophys. Res.,* **87,** 5422–5432.

Kanamori, H., Given, J.W. & Lay, T., 1984. Analysis of seismic body waves excited by the Mount St. Helens eruption of May 18, 1980, *J. geophys. Res.,* **89,** 1856–1866.

Kausel, E., 2006. *Fundamental Solutions in Elastodynamics: A Compendium,* Cambridge Univ. Press.

Kieffer, S.W., 1977. Sound speed in liquid?gas mixtures: Water?air and water?steam, *J. geophys. Res.,* **82,** 2895–2904.

Kim, K., Lees, J.M. & Ruiz, M., 2012. Acoustic multipole source model for volcanic explosions and inversion for source parameters, *Geophys. J. Int.,* **191,** 1192–1204.

Kumagai, H., Mothes, P., Ruiz, M. & Maeda, Y., 2015. An approach to source characterization of tremor signals associated with eruptions and lahars, *Earth Planets Space,* **67,** 178, doi:10.1186/s40623-015-0349-1.

Kundu, P.K. & Cohen, I.M., 2008. *Fluid Mechanics,* 4th edn, Academic Press.

Lighthill, M.J., 1952. On sound generated aerodynamically: I. General theory, *Proc. R. Soc. A,* **211,** 564–587.

Lighthill, M.J., 1954. On sound generated aerodynamically: II. Turbulence as a source of Sound, *Proc. R. Soc. A,* **222,** 1–32.

Lighthill, M.J., 1963. Jet noise, *AAIA J.,* **1,** 1507–1517.

Lighthill, M.J., 1978. *Waves in Fluids,* Cambridge Univ. Press.

Mastin, L.G. *et al.*, 2009. A multidisciplinary effort to assign realistic source parameters to models of volcanic ash-cloud transport and dispersion during eruptions, *J. Volcanol. Geotherm. Res.,* **186,** 10–21.

Matoza, R.S. & Fee, D., 2014. Infrasonic component of volcano-seismic eruption tremor, *Geophys. Res. Lett.,* **41,** 1964–1970.

Matoza, R.S., Fee, D., Garces, M.A., Seiner, J.M., Ramon, P.A. & Hedlin, M. A.H., 2009. Infrasonic jet noise from volcanic eruptions, *Geophys. Res. Lett.,* **36,** L08303, doi:10.1029/2008GL036486.

Matoza, R.S., Fee, D., Neilsen, T.B., Gee, K.L. & Ogden, D.E., 2013. Aeroacoustics of volcanic jets: acoustic power estimation and jet velocity dependence, *J. geophys. Res.,* **118,** 6269–6284.

McKee, K., Fee, D., Yokoo, A., Matoza, R.S. & Kim, K., 2017. Analysis of gas jetting and fumarole acoustics at Aso Volcano, Japan, *J. Volcanol. Geotherm. Res.,* **340,** 16–29.

McNutt, S.R., 1994. Volcanic tremor amplitude correlated with eruption explosivity and its potential use in determining ash hazards to aviation, *U.S. Geol. Surv. Bull.* **2047,** 377–385.

McNutt, S.R. & Nishimura, T., 2008. Volcanic Tremor During Eruptions: Temporal Characteristics, Scaling and Estimates of Vent Radius, *J. Volcanol. Geotherm. Res.,* **178,** 10–18.

Miller, G.F. & Pursey, H., 1955. On the Partition of Energy between Elastic Waves in a Semi-Infinite Solid, *Proc. R. Soc. A,* **223,** 55–69.

Nakahara, H. & Haney, M.M., 2015. Point spread functions for earthquake source imaging: an interpretation based on seismic interferometry, *Geophys. J. Int.,* **202,** 54–61.

Nishimura, T., 1998. Source mechanisms of volcanic explosion earthquakes: single force and implosive sources, *J. Volcanol. Geotherm. Res.,* **86,** 97–106.

Nishimura, T. & Hamaguchi, H., 1993. Scaling Law of Volcanic Explosion Earthquake, *Geophys. Res. Lett.,* **20,** 2479–2482.

Ogden, D.E., Wohletz, K.H., Glatzmaier, G.A. & Brodsky, E.E., 2008. Numerical simulations of volcanic jets: importance of vent overpressure, *J. geophys. Res.,* **113,** B02204, doi:10.1029/2007JB005133.

Petersen, G.N., Bjornsson, H., Arason, P. & von Löwis, S., 2012. Two weather radar time series of the altitude of the volcanic plume during the May 2011 eruption of Grímsvötn, Iceland, *Earth Syst. Sci. Data,* **4,** 121–127.

Pierce, A.D., 1989. *Acoustics: An Introduction to its Physical Principles and Applications,* Acoustical Society of America.

Prejean, S. & Brodsky, E., 2011. Volcanic plume height measured by seismic waves based on a mechanical model, *J. geophys. Res.,* **116,** B01306, doi:10.1029/2010JB007620.

Roach, A.L., Benoit, J.P., Dean, K.G. & McNutt, S.R., 2001. The combined use of satellite and seismic monitoring during the 1996 eruption of Pavlof Volcano, Alaska, *Bull. Volcanol.,* **62,** 385–399.

Rose, L. R.F., 1984. Point-source representation for laser-generated ultrasound, *J. acoust. Soc. Am.,* **75,** 723–732.

Russell, D.A., 1999. Acoustic monopoles, dipoles, and quadrupoles: an experiment revisited, *J. Phys.,* **67,** 660–664.

Senyukov, S., 2013. Monitoring and prediction of volcanic activity in Kamchatka from seismological data: 2000–2010, *J. Volcanol. Seismol.,* **7,** 86–97.

Sparks, R. S.J., Bursik, M.I., Carey, S.N., Gilbert, J.S., Glaze, L.S., Sigurdsson, H. & Woods, A.W., 1997. *Volcanic Plumes,* John Wiley.

Stein, S. & Wysession, M., 2003. *An Introduction to Seismology, Earthquakes, and Earth Structure,* Blackwell Science.

Takei, Y. & Kumazawa, M., 1994. Why have the single force and torque been excluded from seismic source models?, *Geophys. J. Int.,* **118,** 20–30.

Tam, C. K.W., Golebiowski, M. & Seiner, J.M., 1996. *On the two components of turbulent mixing noise from supersonic jets, AIAA Paper*, 96-1716.

Waythomas, C., Haney, M., Fee, D., Schneider, D. & Wech, A., 2014. The 2013 eruption of Pavlof Volcano, Alaska: a spatter eruption at an ice- and snow-clad volcano, *Bull. Volcanol.,* **76,** 862, doi:10.1007/s00445-014-0862-2.

White, R. & McCausland, W., 2016. Volcano-tectonic earthquakes: A new tool for estimating intrusive volumes and forecasting eruptions, *J. Volcanol. Geotherm. Res.,* **309,** 139–155.

Woulff, G. & McGetchin, T.R., 1976. Acoustic Noise from Volcanoes: Theory and Experiment, *Geophys. J. R. astr. Soc.,* **45**, 601–616.

Yamasato, H., 1997. Quantitative analysis of pyroclastic flows using infrasonic and seismic data at Unzen volcano, Japan, *J. Phys. Earth,* **45**, 397–416.

Zobin, V.M., Plascencia, I., Reyes, G. & Navarro, C., 2009. The characteristics of seismic signals produced by lahars and pyroclastic flows: Volcán de Colima, México, *J. Volcanol. Geotherm. Res.,* **179**, 157–167.

APPENDIX A: MONOPOLE AND QUADRUPOLE SOURCES

In the main text we gave details of the seismic force source model and showed that it has similar scaling as the dipole acoustic model. Woulff & McGetchin (1976) also developed monopole and quadrupole models for sound radiation from a plume or jet and here we show the seismic analogies of those models.

For the monopole case, we consider the seismic wave field generated by a point source of volume injection. Aldridge (2002) solved the problem of elastic radiation from a spherical cavity for two different boundary conditions: (1) By prescribing the radial stress on the spherical surface of a cavity and (2) by prescribing the radial displacement on the surface. The two boundary conditions give somewhat different solutions, as shown by eqs (8.9) and (12.11) in Aldridge (2002). Although Aldridge (2002) states the 'mathematical structure of the ... two expressions is identical', the dimensional pre-factors multiplying the common portions of the two solutions are different. The applied pressure or radial stress case has a pre-factor with an energy source term divided by the shear modulus, whereas the applied radial displacement case has a pre-factor only dependent on the injected volume. In addition, Aldridge (2002) states, in reference to the boundary condition of applied radial displacement, that 'the total radiated energy scales linearly with the cavity radius, in contrast to the analogous situation for an applied pressure or radial stress'. Aldridge (2002) also states, in reference to the boundary condition of applied pressure or radial stress, that 'in this case, the total radiated elastic energy scales as the cube of the cavity radius'. Thus, the solutions for the two boundary conditions scale in different ways in terms of radiated energy versus radius. We expect the seismic version of a monopole to correspond to the case of a prescribed radial displacement on the cavity surface. In the far field, the source is described by the rate of volume injection q. The scaling of the far-field particle velocity can be written in terms of mass injection rate $\dot{m} = 2\rho_p q$ as

$$v_M \propto \frac{\omega \dot{m}}{\rho_p \alpha r}, \tag{A1}$$

where ρ_p is the density of the material inside the cavity, r is the distance from the observation point to the source, and particle velocity is denoted as v_M since it is for a seismic monopole. We note that, for volcanic eruptions at the Earth's surface, the source of volume injection is actually a hemisphere instead of a sphere, as shown in Fig. 4. We recognize this difference but assume that the far-field scaling of a hemispherical volume source at the Earth's surface does not vary substantially from a sphere embedded in a whole space. The mass injection rate for this source, $\dot{m} = 2\rho_p q$, has a factor of 2 in its definition since the volume injection is in terms of the surface area of a hemisphere, whereas the volume eruption rate is in terms of the area of the vent, $q = A_v v_e$, which is the intersection of the hemispherical crater with the surface.

We expect that the seismic analogy of the quadrupole case is the result of a moment tensor source model. We adapt the erup-

tion tremor model suggested by McNutt & Nishimura (2008) in which the tremor is generated by pressure disturbances within the conduit. The seismic moment for such a source is given by McNutt & Nishimura (2008) as

$$M = L_c A_v \delta P, \tag{A2}$$

where the geometry of the model is shown in Fig. 4, L_c is the length of the conduit over which the pressure disturbances act, A_v is the area of the vent (or conduit since the geometry is cylindrical), and δP is the fluctuating pressure. As in McNutt & Nishimura (2008), the term moment here is taken to be a scalar moment that multiplies a tensor which represents a cylindrical source volume. For the purposes of exploring scaling, we do not include terms related to the specific form of the tensor. An expression for moment rate $\dot{M} = \omega M$, found by invoking flow described by a Strouhal number in which $\omega \sqrt{A_v} \propto v_e$, is given by

$$\dot{M} \propto \frac{v_e}{R} L_c A_v \delta P, \tag{A3}$$

where v_e is the exit velocity, R is the radius of the conduit, and we've used the fact that $\sqrt{A_v} \propto R$. We further assume that the pressure fluctuation δP is proportional to the dynamic pressure of the plume or jet, $\delta P \propto \rho_p v_e^2$, resulting in

$$\dot{M} \propto \rho_p A_v v_e^3 \frac{L_c}{R}. \tag{A4}$$

Note that this has a similar form as the mass flux source, $\dot{m} = 2\rho_p A_v v_e$, and the force source, $F \propto \rho_p A_v v_e^2$. Each of the three source types is expressed in terms of density of the plume or jet, the vent area, and different powers of exit velocity. The moment source has the additional dimensionless geometrical factor of L_c/R related to the aspect ratio of the seismogenic portion of the upper conduit. In the far field, the particle velocity scales in the following way for a moment source:

$$v_Q \propto \frac{\omega \dot{M}}{\rho \alpha^3 r}, \tag{A5}$$

where we have denoted the particle velocity as v_Q since it is for a seismic quadrupole.

We now consider the scaling of radiated power for the seismic monopole and quadrupole cases. First we analyse the dipole case using a different and simpler technique than shown in the main text to obtain the scaling. In the frequency domain, the far-field particle velocity v from a force source scales as

$$v_D \propto \frac{\omega F}{\rho \alpha^2 r}, \tag{A6}$$

where we have denoted the particle velocity as v_D since it is for a seismic dipole. To analyse the radiated power, we recognize that to within a multiplicative constant, the power is given by

$$W_D \propto \rho \alpha r^2 v_D^2. \tag{A7}$$

Substituting v_D^2 into this equation gives

$$W_D \propto \frac{\omega^2 F^2}{\rho \alpha^3}. \tag{A8}$$

At this point, the specific form of the force source $F \propto \rho_p A_v v_e^2$ can be inserted yielding the dipole scaling we have seen previously:

$$W_D \propto \frac{\rho_p A_v v_e^6}{\alpha^3} \left(\frac{\rho_p}{\rho} \right). \tag{A9}$$

The sixth power dependence on exit velocity agrees with the acoustic dipole scaling in Woulff & McGetchin (1976). By applying the

same procedure to the monopole and quadrupole cases, using the mass injection rate and moment rate sources given above, we obtain the following expressions for radiated power:

$$W_M \propto \frac{\rho A_v v_e^4}{\alpha} \tag{A10}$$

$$W_Q \propto \frac{\rho_p A_v v_e^8}{\alpha^5} \left(\frac{\rho_p}{\rho} \right) \left(\frac{L_c}{R} \right)^2, \tag{A11}$$

where the fourth and eighth power dependencies agree with acoustic scaling in the monopole and quadrupole cases (Woulff & McGetchin 1976). Thus, the seismic analogies of acoustic monopole and quadrupole radiation are given by a volume injection and moment tensor source, respectively.

APPENDIX B: DECOMPOSITION OF A SEISMIC FORCE SOURCE

Here, we consider if a seismic force can be represented by dipoles of explosive and torque sources. We show a detailed derivation for the 2-D case and then describe the general approach and result for 3-D. The geometry of the dipoles in 2-D is shown in Fig. 2: the dipole consisting of an explosion/implosion pair is oriented along the direction of the force and the torque dipole is oriented perpendicular to the force direction. Seismic radiation from an explosion or torque dipole is proportional to the spatial derivative along the direction in which the explosion/implosion or torque/anti-torque pair is offset. For the situation and coordinate system in Fig. 2, this means we take the vertical z-derivative of the explosion, or blast, source and the horizontal x-derivative of the torque source. Expressions for blast (explosion) and torque sources in 2-D are given by Kausel (2006). We seek to find if the sum of these two dipoles is proportional to the Green's function for a seismic force oriented in the vertical direction:

$$C_B \frac{\partial \vec{B}}{\partial z} + C_T \frac{\partial \vec{T}}{\partial x} = (g_{xz}, g_{zz}), \tag{B1}$$

where $\vec{B}$ is the blast (explosion) source, $\vec{T}$ is the torque source, g_{xz} and g_{zz} are the xz- and zz-components of the force Green's tensor, which are used to describe the radiation from a vertically oriented force, and C_B and C_T are proportionality constants to be determined. Note that expressions for the components of the 2-D Green's tensor are also given in Kausel (2006). Although we take the orientation of the force as vertical here, the orientation can be in any direction.

In component form, eq. (B1) can be written as

$$C_B \frac{\partial B_x}{\partial z} + C_T \frac{\partial T_x}{\partial x} = g_{xz} \tag{B2}$$

and

$$C_B \frac{\partial B_z}{\partial z} + C_T \frac{\partial T_z}{\partial x} = g_{zz}. \tag{B3}$$

The blast source is given by (Kausel 2006)

$$\vec{B} = (B_x, B_z) = \frac{-i\omega}{4\mu\alpha} H_1 \left(\frac{\omega r}{\alpha} \right) (\gamma_x, \gamma_z) \tag{B4}$$

where μ is the shear modulus, ω is the angular frequency, α is the P-wave velocity, γ_x and γ_z are components of the unit vector in the radial direction (i.e., direction cosines), and H_1 is the Hankel function of order one. Note that, for brevity, we do not indicate whether the Hankel function is of the first or second kind, since this

distinction will be dependent on the Fourier transform convention. The torque source is given by (Kausel 2006)

$$\vec{T} = (T_x, T_z) = \frac{i\omega}{8\mu\beta} H_1 \left(\frac{\omega r}{\beta} \right) (\gamma_z, -\gamma_x) \tag{B5}$$

where β is the S-wave velocity.

We begin by evaluating eq. (B2). For the term $\partial B_x/\partial z$, we use the following identity for a general function $f(r)$ of the radial coordinate

$$\frac{\partial f}{\partial z} = \frac{\partial f}{\partial r} \gamma_z \tag{B6}$$

and also the following identity for the directional cosine γ_x

$$\frac{\partial \gamma_x}{\partial z} = -\frac{\gamma_x \gamma_z}{r}. \tag{B7}$$

Using these identities, we find that

$$\frac{\partial B_x}{\partial z} = -\frac{i\omega}{4\mu\alpha} \left[\frac{\partial H_1(k_p r)}{\partial r} \gamma_z \gamma_x - H_1(k_p r) \frac{\gamma_x \gamma_z}{r} \right], \tag{B8}$$

where $k_p = \omega/\alpha$. For the term $\partial T_x/\partial x$, we use the following identity for a general function $f(r)$ of the radial coordinate:

$$\frac{\partial f}{\partial x} = \frac{\partial f}{\partial r} \gamma_x \tag{B9}$$

and also the following identity for the directional cosine γ_z

$$\frac{\partial \gamma_z}{\partial x} = -\frac{\gamma_x \gamma_z}{r}. \tag{B10}$$

Using these identities, we find that

$$\frac{\partial T_x}{\partial x} = \frac{i\omega}{8\mu\beta} \left[\frac{\partial H_1(k_s r)}{\partial r} \gamma_x \gamma_z - H_1(k_s r) \frac{\gamma_x \gamma_z}{r} \right] \tag{B11}$$

where $k_s = \omega/\beta$.

We now use the following recursion relations for Hankel functions:

$$\frac{\partial H_1(kr)}{\partial r} = \frac{k}{2} [H_0(kr) - H_2(kr)] \tag{B12}$$

$$H_1(kr) = \frac{kr}{2} [H_0(kr) + H_2(kr)]. \tag{B13}$$

Using these relations on eqs (B8) and (B11) requires combining and organizing them into the following form:

$$\frac{\partial H_1(kr)}{\partial r} - \frac{H_1(kr)}{r} = -k H_2(kr). \tag{B14}$$

We use eq. (B14) and add eqs (B8) and (B11), together with the assumption $C_T = 2C_B$ to find

$$C_B \left(\frac{\partial B_x}{\partial z} + 2 \frac{\partial T_x}{\partial x} \right) = C_B \frac{\omega^2}{\beta^2} \times \frac{i\gamma_x \gamma_z}{4\mu} \left[\frac{\beta^2}{\alpha^2} H_2 \left(\frac{\omega r}{\alpha} \right) - H_2 \left(\frac{\omega r}{\beta} \right) \right]. \tag{B15}$$

Kausel (2006) gives the xz-component of the Green's function as

$$g_{xz} = \frac{1}{\mu} \chi \gamma_x \gamma_z \tag{B16}$$

where

$$\chi = \frac{i}{4} \left[\frac{\beta^2}{\alpha^2} H_2 \left(\frac{\omega r}{\alpha} \right) - H_2 \left(\frac{\omega r}{\beta} \right) \right]. \tag{B17}$$

Compared to Kausel (2006), the right-hand side of eq. (B15) differs from the xz-component of the Green's function g_{xz} by the factor $C_B \omega^2/\beta^2$. Thus, to make the right-hand side of eq. (B15) equal to g_{xz}, the factor C_B must be equal to β^2/ω^2. Based on our earlier

assumption that $C_T = 2C_B$, C_T must be equal to $2\beta^2/\omega^2$. Now we will see if going through the same steps for eq. (B3) leads to the same factors C_B and C_T. If it does, then the combination of blast and torque dipoles with amplitudes determined by these values for C_B and C_T is proportional to a force source.

For the term $\partial B_z/\partial z$ in eq. (B3), we use eq. (B6) and also the following identity for the directional cosine γ_z

$$\frac{\partial \gamma_z}{\partial z} = \frac{1 - \gamma_z^2}{r}. \tag{B18}$$

Using these identities, we find that

$$\frac{\partial B_z}{\partial z} = -\frac{i\omega}{4\mu\alpha} \left[\frac{\partial H_1(k_p r)}{\partial r} \gamma_z^2 + H_1(k_p r) \frac{(1 - \gamma_z^2)}{r} \right]. \tag{B19}$$

For eventual comparison with the expression for the *zz*-component of the Green's function g_{zz} given in Kausel (2006), we rewrite eq. (B19) in terms of Hankel functions of order 0 and 2

$$\frac{\partial B_z}{\partial z} = -\frac{i\omega^2}{4\mu\alpha^2} \left[\frac{H_0(k_p r) + H_2(k_p r)}{2} - H_2(k_p r)\gamma_z^2 \right]. \tag{B20}$$

For the term $\partial T_z/\partial x$ in eq. (B3), we use eq. (B9) and also the following identity for the directional cosine γ_x

$$\frac{\partial \gamma_x}{\partial x} = \frac{1 - \gamma_x^2}{r}. \tag{B21}$$

Using these identities, we find that

$$\frac{\partial T_z}{\partial x} = -\frac{i\omega}{8\mu\beta} \left[\frac{\partial H_1(k_s r)}{\partial r} \gamma_x^2 + H_1(k_s r) \frac{(1 - \gamma_x^2)}{r} \right]. \tag{B22}$$

We rewrite eq. (B22) in terms of Hankel functions of order 0 and 2 for eventual comparison with Kausel (2006) and also in terms of γ_z using $\gamma_x^2 = 1 - \gamma_z^2$ yielding

$$\frac{\partial T_z}{\partial x} = -\frac{i\omega^2}{8\mu\beta^2} \left[\frac{H_0(k_s r) - H_2(k_s r)}{2} + H_2(k_s r)\gamma_z^2 \right]. \tag{B23}$$

Kausel (2006) gives the *zz*-component of the Green's function as

$$g_{zz} = \frac{1}{\mu} \left(\psi + \chi \gamma_z^2 \right), \tag{B24}$$

where χ is given by eq. (B17) and ψ is given by

$$\psi = \frac{i}{4} \left[\frac{H_1(k_s r)}{k_s r} - \frac{\beta^2}{\alpha^2} \frac{H_1(k_p r)}{k_p r} - H_0(k_s r) \right]. \tag{B25}$$

By using the recursion relations for Hankel functions, this equation can be rewritten in terms of Hankel functions of order 0 and 2 as

$$\psi = -\frac{i}{8} \left[H_0(k_s r) - H_2(k_s r) + \frac{\beta^2}{\alpha^2} \left(H_0(k_p r) + H_2(k_p r) \right) \right]. \tag{B26}$$

We need to add eq. (B20) scaled by C_B and eq. (B23) scaled by C_T to verify that the explosion and torque dipoles are proportional to g_{zz}. As done previously, we assume $C_T = 2C_B$ and confirm that it works. We first add the terms in eqs (B20) and (B23) that contain the factor γ_z^2 and use eq. (B17) to obtain

$$C_B \frac{\omega^2}{\beta^2} \frac{\gamma_z^2}{\mu} \frac{i}{4} \left[\frac{\beta^2}{\alpha^2} H_2(k_p r) - H_2(k_s r) \right] = C_B \frac{\omega^2}{\beta^2} \frac{\gamma_z^2}{\mu} \chi \tag{B27}$$

which we identify as $C_B\omega^2/\beta^2$ times the second term on the right-hand side of eq. (B24). We now add the other terms in eqs (B20)

and (B23) and use eq. (B26) to obtain

$$C_B \frac{\omega^2}{\beta^2} \frac{1}{\mu} \frac{-i}{8} \left[H_0(k_s r) - H_2(k_s r) + \frac{\beta^2}{\alpha^2} \left(H_0(k_p r) + H_2(k_p r) \right) \right]$$
$$= C_B \frac{\omega^2}{\beta^2} \frac{1}{\mu} \psi \tag{B28}$$

which we identify as $C_B\omega^2/\beta^2$ times the first term on the right-hand side of eq. (B24). Therefore, for the sum of the scaled versions of eqs (B20) and (B23) to be equal to g_{zz}, C_B must be equal to β^2/ω^2. Since we assumed $C_T = 2C_B$, C_T must be equal to $2\beta^2/\omega^2$. These are the same values for C_B and C_T we obtained when analysing the other component of the Green's tensor, g_{xz}. This means that the seismic wave field radiated by a combination of explosion and torque dipoles scaled by C_B and C_T, respectively, is proportional to the wave field from a force source. The idea that the seismic Green's function for a force source can be represented as the sum of a *P*-wave part and an *S*-wave part has been discussed previously by Nakahara & Haney (2015) and is consistent with the proof shown here involving an explosion dipole (the *P*-wave part) and a torque dipole (*S*-wave part). This completes the demonstration that a seismic force source can be decomposed into dipoles of explosion and torque sources in 2-D.

Finally, we set up the derivation in 3-D but do not go through all the steps shown for 2-D since the 3-D derivation is similar. The geometry of the dipoles is shown in Fig. 3 and, similar to eq. (B1), we seek to find if 3-D explosion (blast) and torque sources satisfy

$$C_B \frac{\partial \vec{B}}{\partial z} + C_T \frac{\partial \vec{T}_1}{\partial x} + C_T \frac{\partial \vec{T}_2}{\partial y} = (g_{xz}, g_{yz}, g_{zz}) \tag{B29}$$

where C_B and C_T are proportionality constants to be determined and g_{xz}, g_{yz} and g_{zz} are components of the 3-D force source. Expressions for the 3-D blast and torque sources are given in Kausel (2006) as

$$\vec{B} = (B_x, B_y, B_z) = \frac{-3i\omega^2}{16\pi\mu\alpha^2} h_1 \left(\frac{\omega r}{\alpha} \right) (\gamma_x, \gamma_y, \gamma_z) \tag{B30}$$

$$\vec{T}_1 = (T_{1x}, T_{1y}, T_{1z}) = \frac{i\omega^2}{8\pi\mu\beta^2} h_1 \left(\frac{\omega r}{\beta} \right) (\gamma_z, 0, -\gamma_x) \tag{B31}$$

$$\vec{T}_2 = (T_{2x}, T_{2y}, T_{2z}) = \frac{i\omega^2}{8\pi\mu\beta^2} h_1 \left(\frac{\omega r}{\beta} \right) (0, \gamma_z, -\gamma_y), \tag{B32}$$

where we have rewritten the expressions in Kausel (2006) in terms of spherical Hankel functions of order 1, shown as h_1. Note that there are two torque sources polarized perpendicular to each other as shown in Fig. 3. Note also that the expression for the blast source in 3-D given by Kausel (2006) agrees with the analogous expression in Ben-Menahem & Singh (1981); the torque source in Kausel (2006) is smaller by a factor of $1/2$ compared to the same source in Ben-Menahem & Singh (1981), reflecting a different convention for defining the amplitude of torque.

The 3-D derivation requires the following recursion relations for spherical Hankel functions:

$$\frac{\partial h_1(kr)}{\partial r} = \frac{k}{3}[h_0(kr) - 2h_2(kr)] \tag{B33}$$

$$h_1(kr) = \frac{kr}{3}[h_0(kr) + h_2(kr)]. \tag{B34}$$

Combining and organizing these relations results in the following useful expression:

$$\frac{\partial h_1(kr)}{\partial r} - \frac{h_1(kr)}{r} = -kh_2(kr), \tag{B35}$$

which is the same in form as eq. (B35) except in terms of spherical instead of normal Hankel functions. With these relations, the 3-D derivation follows the 2-D case closely. Expressions for the 3-D Green's tensor components g_{xz}, g_{yz} and g_{zz} are given in Kausel (2006) and must be rewritten in terms of spherical Hankel functions to facilitate the comparison of terms during the derivation. As a result of this process, we find that $C_B = 4\beta^2/3\omega^2$ and $C_T = 2\beta^2/\omega^2$. Although C_B has a slightly different value than the 2-D case, the consistency of these factors in determining the components g_{xz}, g_{yz} and g_{zz} in eq. (B29) shows that, just as in the 2-D case, a force source can be decomposed into explosion and torque dipoles in 3-D.